Enhancements, Verification, and VMS Integration of VTOL Concept Vehicle Simulation Models

Matthew Gladfelter, Chengjian He, and Hossein Saberi
Advanced Rotorcraft Technology, Inc.
Fremont, CA 94085, USA

David Caudle, Raghuvir Singh, Carlos Malpica, and Christoper Silva
NASA Ames Research Center
Moffett Field, CA 94035, USA

Abstract

Advanced Rotorcraft Technology (ART) and the NASA Ames Aeromechanics branch have jointly developed FLIGHTLAB® simulation models for Advanced Air Mobility (AAM) VTOL concept vehicles. The overarching purpose of the simulation model development is to establish a set of well defined reference vehicles for FLIGHTLAB users and the rotorcraft community. The ongoing research effort and enhancement of these AAM simulation models to fulfill the role of quality reference vehicles is this paper's focus. The content of this paper expands on the established characteristics of these AAM models in three primary areas. First, enhancement of the lift+cruise and tiltwing models with elastic airframe properties is discussed. The process of setting up the elastic airframe model in FLIGHTLAB, as well as the impacts on flight characteristics are explained. The introduction of the elastic airframe modeling allows these models to be used in flight dynamics, loads, and vibration analysis of the configuration designs. Next, linear model generation from the enhanced simulation model is covered. Confirming the validity of the linearized models is of importance, as these linear models are utilized for flight control design and tuning for these experimental configurations. For the final focus, the progress towards implementation of these models into the NASA Ames Vertical Motion Simulator (VMS) is described. This task seeks to demonstrate the procedures of integrating a FLIGHTLAB flight simulation in the VMS environment, test fully integrated simulation with communication between flight dynamics, control, and propulsion models, and explore the essential aspects of simulation model integration in a full flight simulator environment. This includes I/O definition, initialization, trim, flying, etc. By expanding the capabilities of the AAM simulation models, they continue to develop as valuable and approachable modeling references.

Notation

Azi	Acceleration in inertial z-axis
C	Damping matrix
CSGE	Control System Graphical Editor
C_T	Rotor thrust coefficient
DOF	Degree of freedom
F	Vector of total forces
IAS	Indicated airspeed
K	Stiffness matrix
M	Mass matrix
N	Number of rotor blades
P	Vehicle roll rate
Q	Vehicle pitch rate
R	Vehicle yaw rate
r	Non-dimensional blade radial position
VVPM	Viscous Vortex Particle Method
w	Vehicle Z-direction velocity
x_e	Physical degree of freedom
$\vec{w}_{intf}$	Rotor induced interference velocity (off-rotor)
δ_{heave}	Total pilot collective/heave control
δ_{lat}	Total pilot lateral control
δ_{lon}	Total pilot longitudinal control
δ_{ped}	Total pilot pedal/directional control
θ_c	Blade collective pitch angle
θ	Vehicle pitch attitude
ψ	Rotor azimuth
Φ	Eigenvector matrix
η	modal state vector
ζ	Modal damping ratio
ω_e	Modal frequency

[1]Presented at the Vertical Flight Society's 80th Annual Forum & Technology Display, Montréal, Québec, Canada, May 7-9, 2024.

Introduction

The NASA Advanced Air Mobility reference vehicles were designed for the purpose of providing the VTOL/eVTOL community a common set of representative rotorcraft configurations that can support investigation of vehicle technologies, mission requirements, airworthiness, and certification. Incorporating these configurations in the FLIGHTLAB simulation environment allows NASA to further refine their designs and capabilities. From NASA's collection of concepts, three designs were selected for development in FLIGHTLAB, being the lift+cruise, tiltwing, and side-by-side configurations shown in Fig. 1. The characteristics of these designs are outlined in Refs. [1] through [3], while Refs. [4] and [5] describe the missions and research goals that reference vehicles seek to accomplish.

The FLIGHTLAB simulation models were developed to assess the viability of these designs and evaluate the performance and flight dynamic characteristics, while maintaining real-time simulation capabilities. The FLIGHTLAB models were first introduced in Ref. [6], which focused on describing the designs and modeling techniques used. This paper seeks to summarize the research effort performed since the previous publication that expands the modeling capabilities and applications.

VTOL/eVTOL Air Vehicle Models

The vehicle models discussed in this paper reflect the designs available in NASA's public reference vehicle database. The design specifications were acquired from NDARC, Refs. [7], and [8] and OpenVSP, Ref. [9]. The models were generated in FLIGHTLAB's model development system, Ref. [10]. The vehicles discussed are all sized to carry six people. Further details regarding design decisions and specifications are available in Ref. [2] for the lift+cruise and side-by-side configurations, and in Ref. [3] for the tiltwing.

The lift+cruise FLIGHTLAB model, shown in Fig. 2, contains a main wing supporting eight lifting rotors, while a pusher propeller located behind the empennage provides forward thrust. The vehicle model has a total mass of 5791 lbs. Rotors are modeled with blade element formulation and equivalent articulation with stiff flapping dynamics (flap frequency of 1.25/rev). The blade element rotor model consists 12 aerodynamic segments per blade. The airloads are determined from the segment airfoil lift/drag/moment coefficients as a function of local angle of attack, Mach number, and dynamic pressure, plus unsteady effects. The rotor induced inflow is resolved using a three state Peters-He dynamic wake model. Fuselage airloads are calculated from tabulated data provided from NASA CFD runs. Landing gear is modeled with nonlinear spring/damper including ground friction to support start from ground simulation. Blade collective pitch-based control, RPM control, and torque-based control were all explored as viable control schemes. Results discussed in this paper correspond to the torque-based control set up. Control systems were established using FLIGHTLAB's Control System Graphical Editor (CSGE), and contains the logic for low speed rotor-borne flight, higher speed wing-borne flight, and transition between these flight modes. When flight speed exceeds the 85 knot threshold for transition, rotors are stopped, clocked to zero azimuth, and use airloads tables generated from CFD for the stopped rotor. Further information on the FLIGHTLAB model specifications can be found in Ref. [6].

The tiltwing vehicle model consists of eight rotors, of which six are supported with a main, tilting wing and two are supported by a T-tail. The rotors and hubs attached to the T-tail tilt, but the horizontal tail surface is fixed to the body. The FLIGHTLAB model is shown in Fig. 3. The total vehicle weight is 6715 lbs. Each rotor has five blades modeled with blade element formulation. For the tiltwing, rotors are rigid without flapping dynamics - no blade flap or lead-lag DOF was included. Rotor RPM is set for a tip speed of 550 feet per second for low speed and transition, and 300 feet per second for wing borne forward flight. The main wing tilts forward and is the primary lifting surface in forward flight. It is modeled as a rigid structure with 18 aerodynamic segments. The quasi-steady airloads option was used to compute the airloads. The control system was developed in CSGE, and contains rotor collective pitch-based control, control of fixed-wing surface deflections, and transition logic.

The side-by-side model, shown in Fig. 4, has two main rotors supported by structural arms with fairings. The fairing wing is modeled with lifting-line airloads. Rotors are modeled as articulated with blade element formulation and flapping dynamics. Blades contain 20 aerodynamic segments. The tail is modeled as an inverted V-tail to provide longitudinal and directional stability. Control is defined in CSGE using collective pitch-based control of the main rotors and deflection of the ruddervators.

Each of these FLIGHTLAB vehicles incorporates interference models developed as part of the research focus of Ref. [6]. Interference tables were constructed from Viscous Vortex Particle Method (VVPM) data to retain the important characteristics of the interference while maintaining real-time capabilities. The lift+cruise and tiltwing models feature rotor-on-rotor interference extracted via this method, while the

side-by-side model contains both rotor-on-rotor and rotor-on-empennage interference. Figure 5 shows an example of the VVPM wake data used to generate these interference tables.

With these well defined simulation models and FLIGHTLAB rotorcraft analysis capabilities, the primary objectives of the research effort were able to be accomplished. The following sections describe how these models were further enhanced and utilized to demonstrate their usefulness in modal/vibration analysis, linear model generation, and real-time simulation environment integration.

Enhancement with Elastic Airframe

The first model enhancement task pursued was adding elastic airframe properties. Incorporating these properties allows the simulation model to capture the elastic motion within the airframe, which allows for vibration studies not possible with a rigid model. To demonstrate implementation of elastic properties, NASA generated NASTRAN modal data for the lift+cruise vehicle and the tiltwing vehicle in the fixed-wing cruise condition. The given elastic properties correlate to the entire airframe excluding the rotors.

The finite element modal analysis output of a program such as NASTRAN includes modes and modeshapes or eigenvalue and eigenvectors for a specified frequency range. These modes are the results of linear analysis and are valid for small to moderate deformations. For the FLIGHTLAB model, the total response of the vehicle is determined as the sum of the large rigid body motion plus the small to moderate elastic deformations. The 3D finite element dynamic equation of motions starts with equation 1

$$M\ddot{x}_e + C\dot{x}_e + Kx_e = F \tag{1}$$

Where x_e is the physical degree of freedom, M, C and K are mass, damping and stiffness matrices, and F is the force vector. The force vector F consists of aerodynamic, gravitational, and other external forces. The eigenvalue and eigenvector or modes and modeshapes of the finite element model are computed by performing eigenanalysis on only the M and K matrices. The C matrix is excluded and therefore the resulting modes are real. Assuming Φ is the eigenvector matrix and η is the modal state vector, the physical states may written as a linear combination of modal states as in equation 2. By replacing x_e in Equation 2 with equation 1, the transformation to the modal space is achieved and is presented in equation 3.

$$x_e = \Phi\eta \tag{2}$$

$$\ddot{\eta} + 2\zeta\omega_e\dot{\eta} + \omega_e^2\eta = \Phi_{es}^T F \tag{3}$$

The following steps are taken to create and solve airframe elastic response. First, a rigid body model is formed with the load paths to the nodes of interest. The nodes of interests are the ones to which the load generating components such as a rotor or sensors are connected. An elastic airframe module is defined that solves the modal Equation 3 and computes elastic deformation via Equation 2. The basic inputs to this module are ζ. ω_e, Φ and F. ζ is the modal damping ratio and usually is used to include structural damping. If there is no estimation for ζ, a value around 1% may be considered, which was done so for the NASA AAM models. The modal frequency ω_e and eigenvector matrix Φ are available from eigenanalysis. The modal equation is solved in the elastic airframe module and nodal elastic motion is computed using modal states and their derivatives. These motions are passed to the elastic joints. Each elastic joint element adds the elastic motion to the rigid body motion of the node, and passes the total to the load generating components (rotors). Load generating components use the total motion to compute their loads. Next, load generating components compute their loads, and pass them to the elastic joints. The elastic joints pass the loads to the elastic airframe module as well as to the nodes of rigid body. The computation of Equations 2 and 3 are performed in the elastic airframe module. This approach is effective in computing both elastic and rigid body motion, and ensuring both are propagated accurately throughout the model components.

The lift+cruise model NASTRAN data consisted of modal analysis for 72 nodes and 20 modes. The first six modes corresponded to the 6 DOF rigid body that are already included in the model, and therefore were excluded from the elastic airframe model. Figure 6 shows the NASTRAN model. The data is organized in nine groups of eight nodes, that encircle the rotor boom near the respective rotor attachment point. Figure 7 shows a set of selected nodes at one of the rotor booms. Only one node for each rotor is utilized, so for the forward, low mounted rotors, the lowest node data was used for connecting the rotors. For the aft, high mounted rotors, the highest node data was used. To account for the distance between each rotor hub center and corresponding NASTRAN node a rigid bar was added.

The NASTRAN modal data for the tiltwing model in cruise consisted of 32 nodes and 20 modes. The model is shown in Figure 8. The NASTRAN data contains information for nodes in groups of four around the nacelle near each rotor attachment (Fig. 9). Only one node is needed for each rotor connection. As such, using one of the four nodes and using averaged values from the four nodes were considered. Inspection of the tiltwing NASTRAN data revealed that between the four nodes of each group, modeshape values were close to each other, so an averaged value of the four NASTRAN nodes is used.

The elastic airframe data tables were constructed for each model from the mode shape data, with proper unit conversions and reference frame transformation for the FLIGHTLAB body frame. The modal elastic fuselage option was enabled and the modal data table was assigned, thus setting up the enhanced aeroelastic models for these configurations. To ensure that the elastic airframe modal data was properly integrated into the current model, several verification checks were performed. The first series of checks involved the comparison of the modal frequencies and the modeshapes at the rotor connection nodes (elastic joints). With rotor blade mass and chord at very low values, an eigenanalysis was performed and modal frequencies were obtained. Figure 10 shows the root location of some of the rigid body modes and one of the elastic modes of the lift+cruise model. The resulting frequency of 24.0742 from the simulation compares very well with the NASTRAN frequency of the corresponding mode which is 24.075. The real part of the eigenvalue (-0.4815) reflects the 1% damping ratio assigned to the mode. The check was repeated for several other modes. Some of the results are shown in Table 1.

Table 1: Modal Frequency Verification

	NASTRAN Frequency (rad/s)	FLIGHTLAB Frequency (rad/s)
Mode 1	24.075	24.075
Mode 7	86.423	86.423
Mode 14	156.06	156.06

Next, the implementation of the mode shapes was checked. For this, the model was oriented at zero pitch, roll, and yaw angles. This was done to make the simulation coordinates match the coordinates of the NASTRAN modeshape and allow for direct comparison of the modeshapes. The elastic modal state was set to the value of one and the input was propagated though the model. Afterward, the nodal deformations were extracted and compared with the NASTRAN modeshapes. Table 2 shows the NASTRAN translational and rotational modeshapes for one rotor connection node for mode 7 and the corresponding deformations of the elastic joints from the simulation. Mode 7 is the first elastic mode of the airframe. The simulation matched the modeshapes of NASTRAN output, verifying the setup. This check was also performed for several other modes to ensure proper integration of the elastic airframe. These verification steps were performed for both the lift+cruise and tiltwing implementations.

Table 2: Modeshape Verification for First Elastic Mode

	NASTRAN Modeshape (ft) [x,y,z]
Rotor 1 Node	[1.8201e-03, -3.8159e-03, 1.4480e-02]
	NASTRAN Modeshape (rad) $[\phi, \theta, \psi]$
Rotor 1 Node	[-2.5143e-03, -1.0674e-03, 2.1691e-04]
	Simulation Deformation (ft) [x,y,z]
Rotor 1 Node	[1.8201e-03, -3.8159e-03, 1.4480e-02]
	Simulation Deformation (rad) $[\phi, \theta, \psi]$
Rotor 1 Node	[-2.5143e-03, -1.0674e-03, 2.1691e-04]

Vehicle trim characteristics were evaluated to check for effects from the inclusion of elastic properties. Trim characteristics were assessed for the lift+cruise model via a trim sweep from 0 to 120 knots in 10 knots intervals. The rigid model was run first to establish the trim trends for the model prior to aeroelastic enhancement. The elastic model was setup and run with the first 14 elastic modes. Both the rigid and elastic models contain the interference. For the low speed rotor-borne mode, pitch attitude was fixed and pusher propeller collective was used as a trim variable, while for the high speed wing-borne mode, pitch attitude was included as a trim variable. Figure 11 shows the resulting trimmed control locations for sweep while Fig. 12 shows two of the important trim outputs, being vehicle pitch attitude and power required. The trim controls and results show that trim behavior is suitable for the vehicle and that the introduction of the elastic airframe properties does not significantly impact the trim solution.

Similar conclusions were drawn from the tiltwing trim sweep. The current modal elastic data set generated by NASA for the tiltwing configuration is applicable only for the wing-borne forward flight mode with main wing at zero degrees tilt. As such, the trim analysis comparison was constrained to this flight range. The tiltwing model with and without the elastic enhancement was trimmed for airspeeds of 110 to 180 knots level forward flight, and trim variables were collected. Both models include the interference. Trim

controls are presented in Figure 13 and additional trim results are in Figure 14. The plots show that differences in trim characteristics between models were small. Trim converged successfully, so no adjustments to control logic were needed.

Flight dynamics were also compared between rigid body and elastic airframe models. Flight dynamic assessment is important in determining if the fuselage support flexibility influences the flight characteristics. The frequency domain response of each vehicle and control channel was investigated for impacts of the flight characteristics. Figure 15 shows the longitudinal frequency response for the tiltwing at cruise. The Bode plots for the vehicle with and without the elastic airframe enhancement show very little difference. It was concluded that the inclusion of the current set of elastic airframe properties has negligible impact on the flight dynamics.

The research performed has shown how elastic properties are integrated into the AAM simulation models, and how this implementation is verified. Analysis of the trim and flight dynamics shows that these flight characteristics are not largely influenced by the inclusion of the elastic properties. This enhancement of the vehicle models with the airframe elastic properties further improves the accuracy of the simulation to the real world counterpart, and allows for future analysis of critical engineering considerations, such as vibration and modal analysis.

Linear Model Generation and Validation

The next major objective for the AAM simulation models was to generate linear models. A linear model is a matrix representation of the nonlinear flight dynamics for a given flight condition, and can be used to expedite control design, provided the linear model is accurate. Thus an important objective of this task was verifying that the generated linear models effectively capture the nonlinear flight dynamics.

Linear models were generated via the perturbation method, in which the partial derivatives of the residuals of generalized equations with respect to states and control inputs are computed. Linear model equations are of the state space form:

$$\{\dot{\boldsymbol{X}}\} = [\boldsymbol{F}] * \{\boldsymbol{X}\} + [\boldsymbol{G}] * \{\boldsymbol{U}\} \tag{4}$$

$$\{\boldsymbol{Y}\} = [\boldsymbol{H}] * \{\boldsymbol{X}\} + [\boldsymbol{D}] * \{\boldsymbol{U}\} \tag{5}$$

For these equations, $\{X\}$ is the state vector, $\{U\}$ is the control input vector, and $\{Y\}$ is the vector of selected outputs. In the above equations, matrix $[F]$ is the stability or dynamic matrix, $[G]$ is the control matrix, $[H]$ is the output matrix, and $[D]$ is the direct input matrix. For these nonlinear systems, the matrices vary with flight condition. As such, both full order and reduced order linear models were generated at several conditions of interest, and are applicable for analysis only near these conditions.

Reduced order linear models are determined by quasi-static reduction of the full-order model. Reduced order models allow for smaller sized matrices while retaining the dynamically significant states. For example, the lift+cruise reduced order linear model retains the nine body states and eight motor shaft degrees of freedom corresponding to the rotor speed of each lifting rotor. The simplicity of the reduced order linear model makes it suited for control design. The flight dynamics of the full order model are included in results as a comparison check.

For each of the designs, linear models were generated via the FLIGHTLAB development system linearization tools. To assess the linear model accuracy, both the time domain and frequency domain flight dynamic response were compared to the nonlinear model. Starting with the lift+cruise model, the results of the linearized flight dynamics model are presented in Figures 16 through 23. These results are derived from the torque-controlled model, with reduced order linear model having 17 states (9 body states, 8 lifting rotor speed states). First, a time domain check of the flight dynamics was performed by exciting each control channel individually with a five percent doublet input. Vehicle attitude, rate, and translation velocity response is recorded and compared between the nonlinear, full order linear, and reduced order linear models at several flight conditions. Figure 16 shows the response results for a longitudinal control stick doublet input at the hover flight condition. The primary pitch rate response of the linear model follows the nonlinear trend well through the first peak, with small deviation in the pitch rate and fore-aft body velocity response as time goes by. An example for the lateral time-domain response at 80 knots level forward flight, Fig. 17, shows that good fitting of the flight dynamics is achieved by the linear model for the pilot input, while some of the higher frequency content is not captured by the reduced order model states.

Frequency domain flight dynamic results were generated by exciting a given control input with a ninety second frequency sweep. The sweep is structured to cover the frequency range of 0.5 to 50 radians per second, to capture the frequencies of interest for flight dynamics applications (1 to 10 rad/s). The resulting response of the vehicle rate was then converted into the frequency domain as a Bode plot. Figure 18 shows

the resulting lift+cruise Bode plot for the longitudinal response at hover. The nonlinear response shows good coherence, and the reduced order linear model response matches the nonlinear response well, especially in the one to ten radians per second frequency range. Similar accuracy was achieved for the other control channels at hover, verifying that the linear model is suitably accurate for control design. A full set of four channel responses is provided for the 40 knot level flight condition as Figures 19 through 22. This rotor-borne transition airspeed provides a response set that illustrates the flight dynamics of the model and shows some of the linearization limitations being investigated. The Bode plots show that the full order and reduced order linear models provide an excellent match to the nonlinear response at high coherence frequencies above two radians per second. At lower frequencies, some discrepancies between models is observed. The difference is most notable in the heave response, and is attributed to the linearization method's limited ability to capture the effects introduced by the rotor-on-rotor interference model. Thus, from the frequency domain analysis one can conclude that the linear models are suitable for capturing a majority of the flight dynamics of interest, but are limited in their usefulness in low frequency analysis for transition airspeeds where the interference effect is notable. Once the vehicle has fully transitioned to its wing-borne mode, the linear model flight dynamics match the nonlinear set well. The longitudinal response at 120 knots is provided as Fig. 23.

Linear models were similarly generated for the tiltwing and side-by-side models, with model verification ongoing. For these vehicles, time domain checks of the linear model flight dynamics matched their nonlinear counterparts well. The tiltwing time domain longitudinal doublet response for hover is shown in Fig. 24. The reduced order linear model captures the response of the first peak well, with some deviation in the transient response. The longitudinal frequency domain response is shown in Fig. 25, with the only discrepancies occurring around one radian per second where the nonlinear model coherence is lower. The other control channels were similarly verified for the tiltwing at hover. Frequency domain verification of linear models for tiltwing and side-by-side at 40 knot intervals is ongoing. The culmination of this task will represent a significant step forward in the development of these designs, as the availability of the linear models is a valuable asset in study and design refinement.

NASA Vertical Motion Simulator Integration

In addition to model enhancements and linearization, ART and NASA are seeking to integrate the AAM simulation vehicle models in the VMS (Fig. 26). This task includes several goals. Starting with the lift+cruise model, the task will demonstrate the procedure of integrating a FLIGHTLAB run-time model in the VMS environment. This process will establish and test the communication between the host, the flight model, and additional control and propulsion modules of NASA's design. The demonstration also seeks to address the significant technical details of establishing initial conditions, trimming, and performing maneuvering flight. Complete integration of the model in the VMS will allow for further study of the flight and handling properties of these designs in the real-time environment. While past joint efforts between ART and NASA, such as Ref. [14], have resulted in successful integration of FLIGHTLAB flight models, integration of the AAM vehicles offers a unique opportunity to streamline the process and explore the challenges associated with these advanced designs.

The key technical challenge with VMS integration is ensuring proper data communication between components by a means that is real-time viable. Figure 27 presents the diagram of data connection between critical modules. As previously mentioned, the ability to support NASA-defined control and propulsion modules is important for future design refinement, so the host environment must be set up to communicate with these along with the FLIGHTLAB-generated run-time model. To organize the data communication structure, groups of variables were assigned to connections outlined in Fig. 28. The required variables for these connections were considered for initialization, trim, and real-time maneuver to ensure each process of simulation could be performed successfully. Special consideration is being applied to address how the requirements of torque-control and associated time delays are handled for these processes.

With a high-fidelity flight dynamics model integrated into the VMS, NASA is able to improve its capability to investigate the handling and ride qualities of advanced vehicle configurations in hover and low speed (Ref. [15] through [17]), as well as conduct research in forward and transition flight. Along with higher fidelity flight dynamics models, augmentation control laws can be developed using the generated linear models and integrated into the VMS as the control module. System identification techniques, such as those described in Ref. [18] and [19], are used to

design the control module from the linear models. Both the flight control and propulsion modules are being developed by NASA in Simulink, which can then be converted to C-code to run in the VMS. Research performed by Malpica et al. (Ref [15]) shows the need for an accurate propulsion model, particularly for rpm-controlled vehicles, as handling qualities were shown to deteriorate significantly during aggressive maneuvers. Successfully integrating the FLIGHTLAB run-time model with the VMS architecture and communicating with independently developed propulsion and flight control modules will enhance NASA's ability to better asses the handling and flight characteristics of these designs.

The VMS host environment will perform the trim algorithm, while the established data exchange ensure synchronization of states between modules. Aspects of the trim process are covered in Ref. [20]. The run-time model will support suspending integration of the aircraft body degrees of freedom to accommodate the trim process.

To facilitate integration, the lift+cruise FLIGHTLAB run-time model was generated along with utilities to establish communication with the host. The FLIGHTLAB run-time model (FCM file) can be generated from the FLIGHTLAB development system model, allowing the FLIGHTLAB user to easily iterate on the design. The run-time model retains the flight dynamic model structure and run-time data of the development system model. The FCM library consists of a set of Application Programming Interface (API) functions that enable the integration of run-time model within a real time flight simulation environment. The run-time model is delivered alongside the FCM Library to ensure operation within the VMS host simulator. A C-code wrapper is used to further facilitate the use of FCM API utility in support of VPM integration. The C-code wrapper includes the header file and environment setup for proper data connections, run-time model execution, etc.

The FLIGHTLAB run-time model was set up in ART's NovaSim for preliminary hands on testing. For these simulation tests, a basic mixer for pilot control inputs derived from NDARC specifications, along with a SAS were incorporated into the run-time model. Following minor adjustment to the longitudinal mixer gain, the simulation model was found to exhibit suitable handling qualities for pilot controlled flight. Take off, hover, and transition through rotor-stop were among the maneuvers tested (Fig. 29).

Integration with the VMS is ongoing. At present, a lift+cruise run-time model that includes control and propulsion components based on the torque-controlled setup has been integrated and is undergoing testing of communication channels and real-time capability. The NASA-developed control and propulsion modules will be included upon completion of these tests.

Summary and Conclusions

ART and NASA have developed FLIGHTLAB simulation models for the lift+cruise, tiltwing, and side-by-side AAM reference vehicle designs, and are continuing to expand on the features and uses of these models. This paper provides an overview of three areas of development for these models.

Elastic airframe properties were included in the lift+cruise and tiltwing models. The introduction of these properties demonstrates how elastic enhancements can be applied to VTOL simulation models. Furthermore, the inclusion of elastic airframe properties allows for these reference vehicles to be used to analyze airframe flexibility on flight dynamics, and support modal and vibration analysis.

Next, the approach for linear model generation was defined, and analysis of the linear model responses in comparison to nonlinear model counterparts was explored. The results show that the linear models are suitable for capturing the flight dynamics of interest, with some limitations introduced by the linearization method in resolving rotor interference effect in transition flight. These linear models will prove valuable tools for refining the control design of these configurations.

Finally, the progress towards integrating these models in NASA's VMS was addressed. The ongoing goals of the task are to establish a streamline process for run-time model integration, and support flight and handling quality assessment in the real-time VMS environment. A top level overview of the communication between the VMS host environment and the run-time model was covered, which supports the inclusion of external control and propulsion modules. The integration of the lift+cruise model is underway to demonstrate the process.

These areas of development expand the capabilities of these AAM reference vehicle models and demonstrate their usefulness in engineering analysis. As their modeling capabilities continue to be enhanced, these simulation models provide a valuable resource for FLIGHTLAB users, and a useful component in supporting NASA's goal of enabling community innovation via the reference vehicle fleet.

Acknowledgment

This research was sponsored by the NASA SBIR program under contract 80NSSC21C0610, with Carlos Malpica (Aeromechanics Office, NASA Ames) as the technical monitor.

References

[1] Wayne Johnson, Christopher Silva, and Eduardo Solis. "Concept Vehicles for VTOL Air Taxi Operations," *AHS Technical Conference on Aeromechanics Design for Transformative Vertical Flight*, San Francisco, CA, January 2018.

[2] Christopher Silva, Wayne Johnson, Kevin Antcliff, and Michael Patterson. "VTOL Urban Air Mobility Concept Vehicles for Technology Development," *2018 Aviation Technology, Integration, and Operations Conference*, Atlanta, GA, June 2018.

[3] S. Whiteside, B. Pollard, K. Antcliff, N. Zawodny, X. Fei, C. Silva, and G. Medina. "Design of a Tiltwing Concept Vehicle for Urban Air Mobility," NASA STI Program Report Series, NASA/TM-20210017971, June 2021.

[4] M.D. Patterson, K.R. Antcliff, and L.W. Kohlman. "A Proposed Approach to Studying Urban Air Mobility Missions Including an Initial Exploration of Mission Requirements," *AHS International 74th Annual Forum and Technology Display*, Phoenix, AZ, 2018.

[5] K.R. Antcliff, S. Whiteside, L.W. Kohlman, and C. Silva. "Baseline Assumptions and Future Research Areas for Urban Air Mobility Vehicles," *AIAA SciTech Forum and Exposition*, Dallas, TX, 2019.

[6] Matthew Gladfelter, Chengjian He, Hossein Saberi, Carlos Malpica, Wayne Johnson, and Christopher Silva. "Enhanced Flight Dynamics Models with Aerodynamic Interference for Real-Time Simulation of VTOL Concept Vehicles," *Vertical Flight Society 79th Annual Forum*, West Palm Beach, FL, May 2023.

[7] Wayne Johnson. "NDARC NASA Design and Analysis of Rotorcraft," *NASA/TP-2015-218751*, NASA, Moffett Field, CA, 2015.

[8] Wayne Johnson. "NDARC NASA Design and Analysis of Rotorcraft - Theory," NASA, Moffett Field, CA, April 2019.

[9] Robert A. McDonald and James R. Gloudemans. "Open Vehicle Sketch Pad: An Open Source Parametric Geometry and Analysis Tool for Conceptual Aircraft Design," *AIAA 2022-0004, AIAA SciTech 2022 Forum*, January 2022.

[10] Du Val, R. and He, Chengjian,"FLIGHTLAB Modeling for Real-Time Simulation Applications," International Journal of Modeling, Simulation, and Scientific Computing, Vol. 8, No. 4, 2017.

[11] Chengjian He and J. Zhao. "Modeling Rotor Wake Dynamics with Viscous Vortex Particle Method," *AIAA Journal*, 47(4), April 2009.

[12] Chengjian He and N. Rajmohan. "Modeling the Aerodynamic Interaction of Multiple Rotor Vehicles and Compound Rotorcraft with Viscous Vortex Particle Method," *American Helicopter Society 72nd Annual Forum*, West Palm Beach, FL, May 2016.

[13] J. Kim, Chengjian He and Jan Goericke. "Modeling and Analysis of eVTOL Air Vehicle Interactional Aerodynamics and Mission Performance," VFS Aeromechanics for Advanced Vertical Flight Technical Meeting, San Jose, CA, January 21-23, 2020.

[14] Chengjian He, Mun Hong Lim, and Dave Mitchell. "Simulation Support for Development of ADS-33 Specifications for Heavy Lift Rotorcraft," *American Helicopter Society 65th Annual Forum*, Grapevine, TX, May 2009.

[15] Carlos Malpica, et. al. "Handling Qualities of Multirotor RPM-Controlled Electric-Vertical Take-Off and Landing (eVTOL) Aircraft for Urban Air Mobility (UAM)," *Vertical Flight Society 79th Annual Forum*, West Palm Beach, FL, May 2023.

[16] Jeremy Aires, Shannah Withrow-Maser, Allen Ruan, Carlos Malpica, Stefan Schuet. "Analysis of Handling Qualities and Power Consumption for Urban Air Mobility (UAM) eVTOL Quadrotors with Degraded Heave Disturbance Rejection and Control Response," *Vertical Flight Society 78th Annual Forum*, Ft. Worth, TX, May 2022.

[17] George Altamirano, Justin Matt, John Foster, Peter Suh, Curtis Hanson, Carlos Malpica, Stefan Schuet. "Flying Qualities Analysis and Piloted Simulation Testing of a Lift+Cruise Vehicle with Propulsion Failures in Hover and Low-Speed Conditions," *Vertical Flight Society 79th Annual Forum*, West Palm Beach, FL, May 2023.

[18] Tom Berger, Mark Lopex, Aaron Wagner, Mark Tischler. "Guidelines for System Identification of Multirotor Vehicles with Highly Correlated Inputs," *Vertical Flight Society 76th Annual Forum*, Virginia Beach, VA, Oct 2020.

[19] Samuel Nadell, Tom Berger, Christopher DiMarco, Mark Lopez. "System Identification and Stitched Modeling of the ADAPT™Winged Compound Helicopter Scaled Demonstrator," *Vertical Flight Society 78th Annual Forum*, Ft. Worth, TX, May 2022.

[20] Richard E. McFarland. "Trimming an Aircraft Model for Flight Simulation," NASA Technical Memorandum 89466, Moffett Field, CA, Oct 1987.

(a) Lift+Cruise

(b) Tiltwing

(c) Side-by-side

Figure 1: Advanced Air Mobility (AAM) VTOL Concept Vehicles

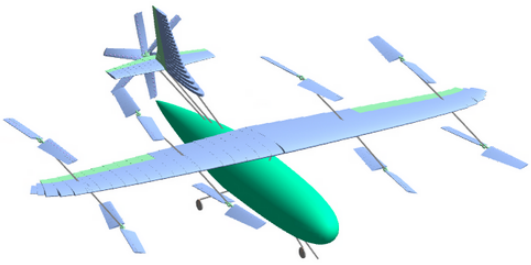

Figure 2: Lift+Cruise FLIGHTLAB Vehicle Model

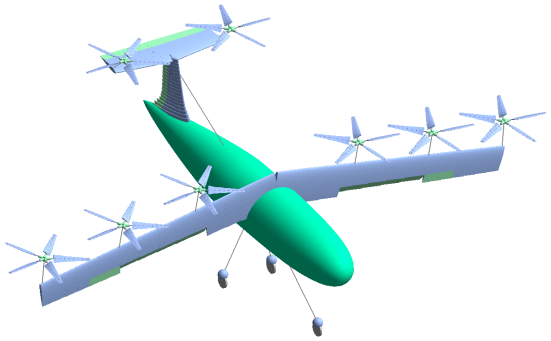

Figure 3: Tiltwing FLIGHTLAB Model in Hover

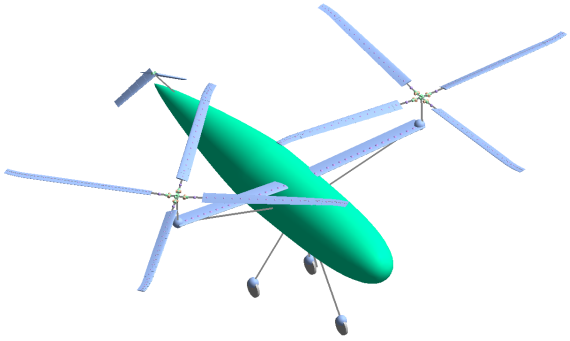

Figure 4: Side-by-side FLIGHTLAB Vehicle Model

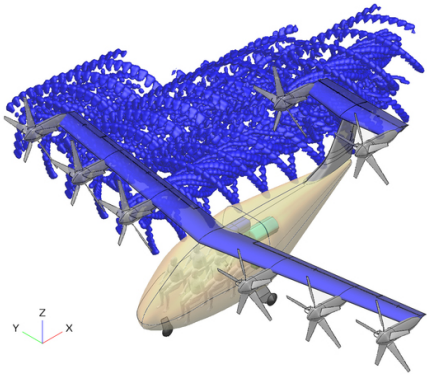

Figure 5: Tiltwing Configuration with VVPM Wake Overlay

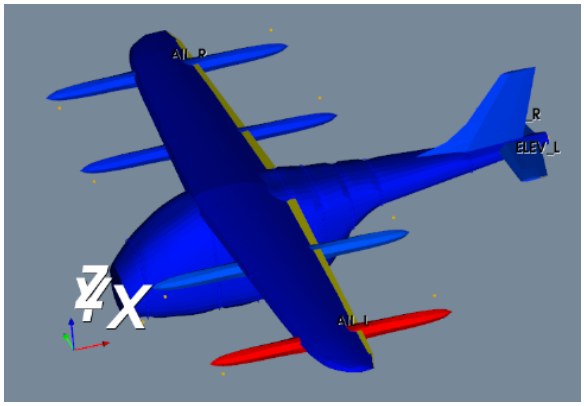

Figure 6: Lift+Cruise NASTRAN Elastic Airframe Model

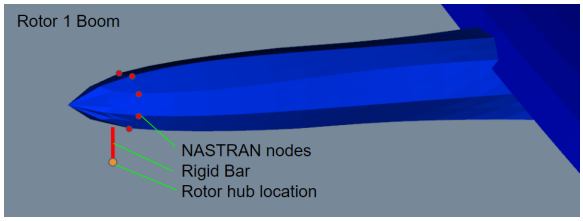

Figure 7: Lift+Cruise Node Locations for Rotor 1 Boom

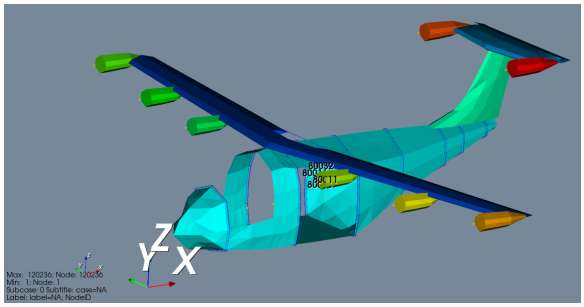

Figure 8: Tiltwing NASTRAN Elastic Airframe Model

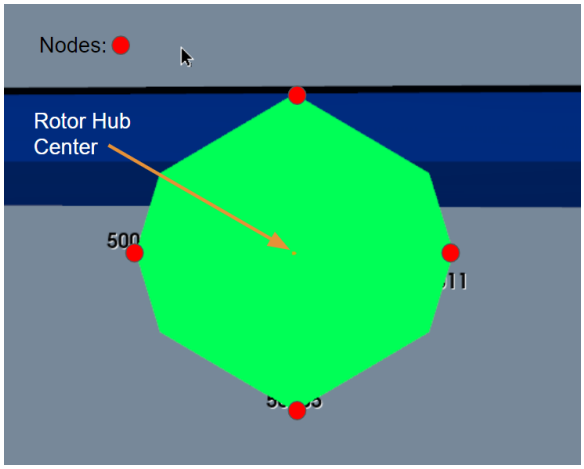

Figure 9: Front View of Tiltwing Node Locations for Rotor 3

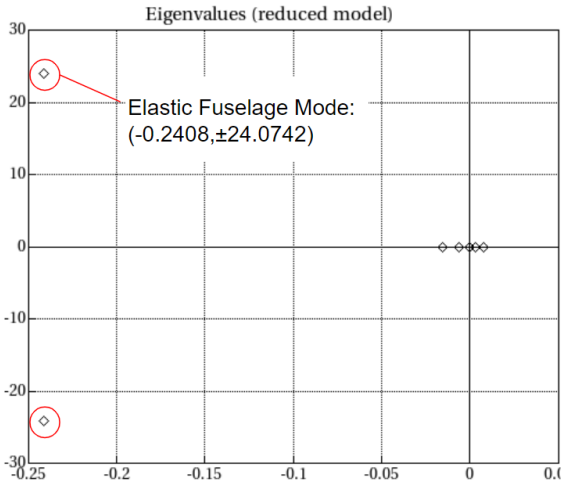

Figure 10: Lift+Cruise Eigenanalysis of an Airframe Mode

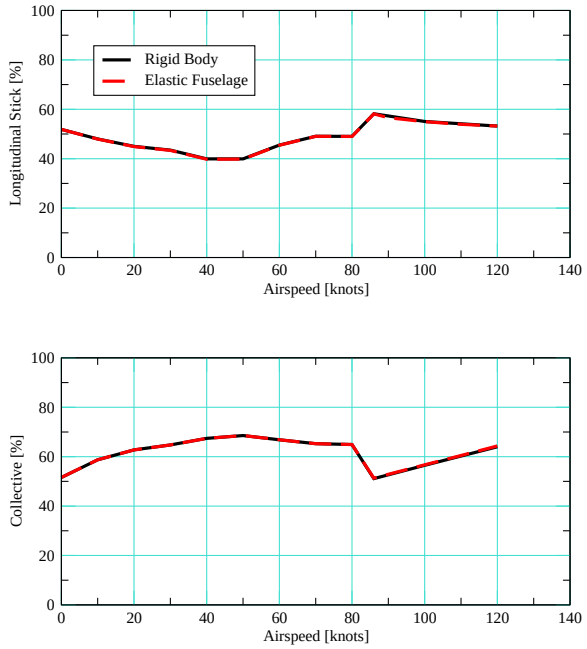

Figure 11: Lift+Cruise Trim Controls for Rigid and Elastic Airframe Models

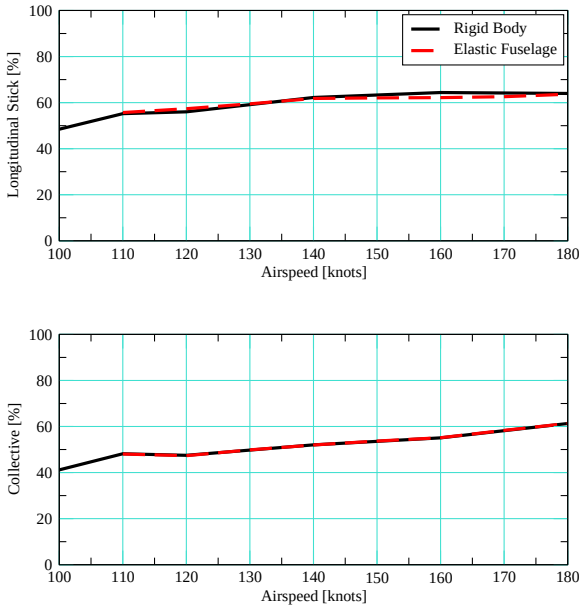

Figure 13: Tiltwing Trim Controls for Rigid and Elastic Airframe Models

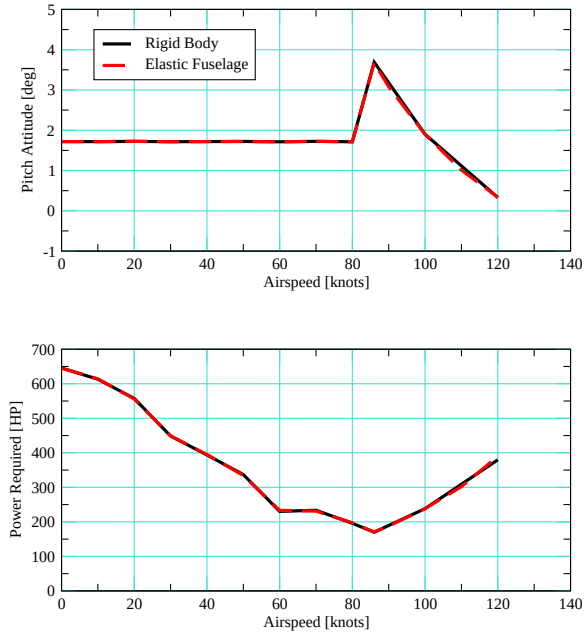

Figure 12: Lift+Cruise Trim Results for Rigid and Elastic Airframe Models

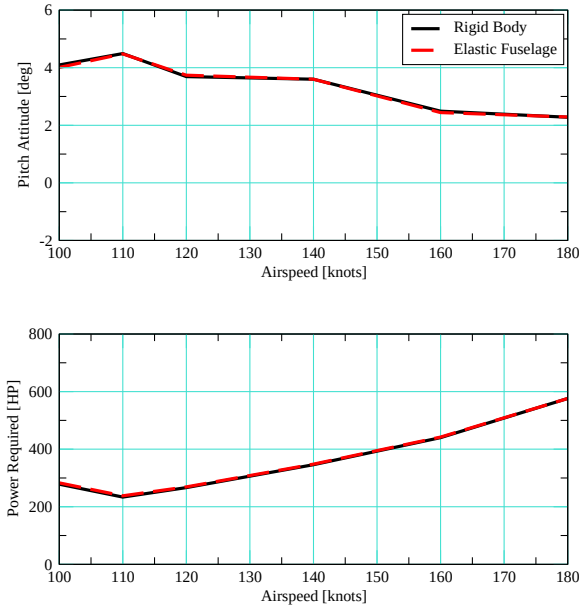

Figure 14: Tiltwing Trim Results for Rigid and Elastic Airframe Models

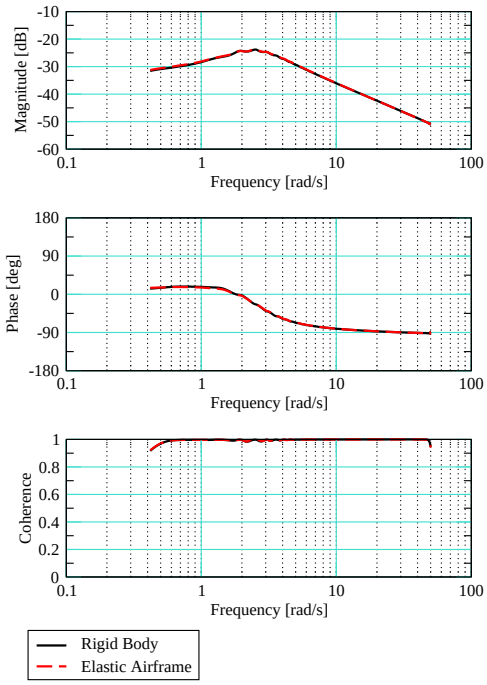

Figure 15: Frequency Domain Response to Tiltwing Longitudinal Input at 150 knots

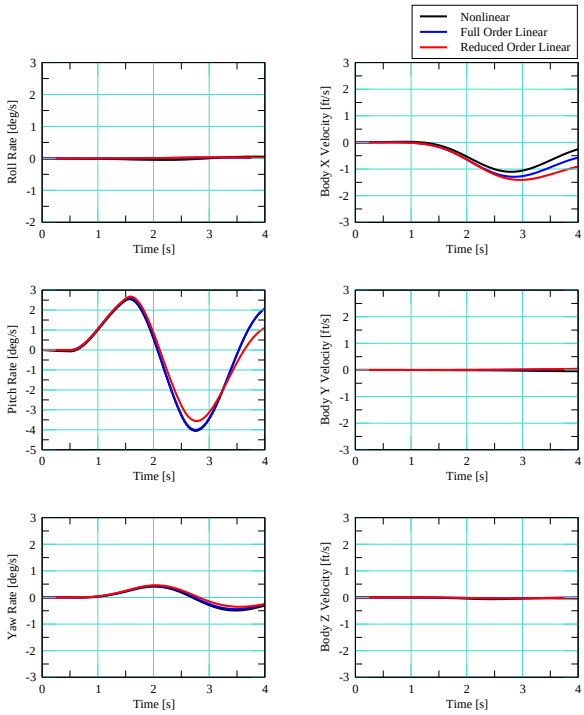

Figure 16: Torque-Controlled Lift+Cruise Doublet Response to Longitudinal Input at Hover

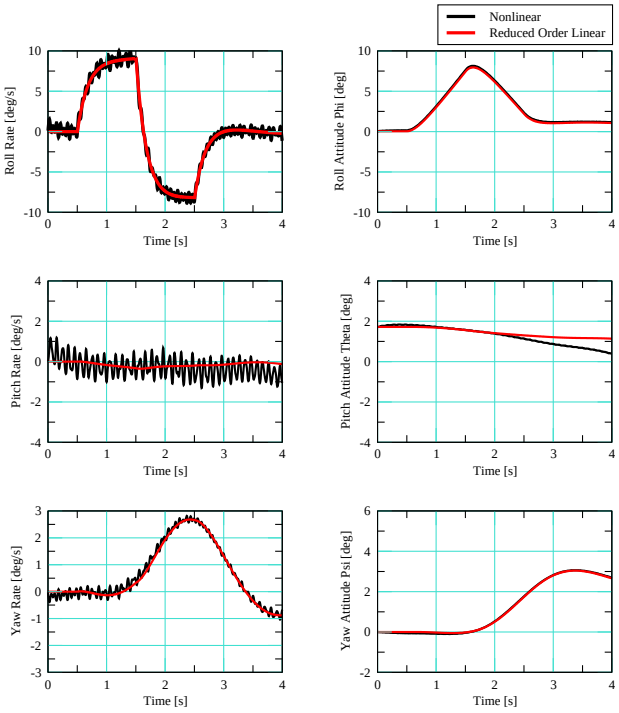

Figure 17: Torque-Controlled Lift+Cruise Doublet Response to Lateral Input at 80 Knots

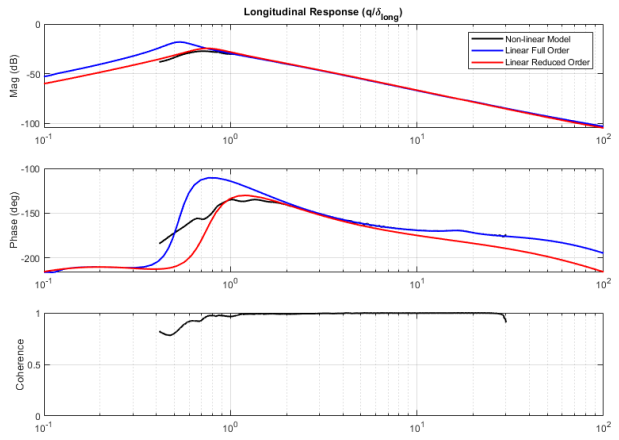

Figure 18: Torque-Controlled Lift+Cruise Frequency Response to Longitudinal Input at Hover, Q/δ_{lon}

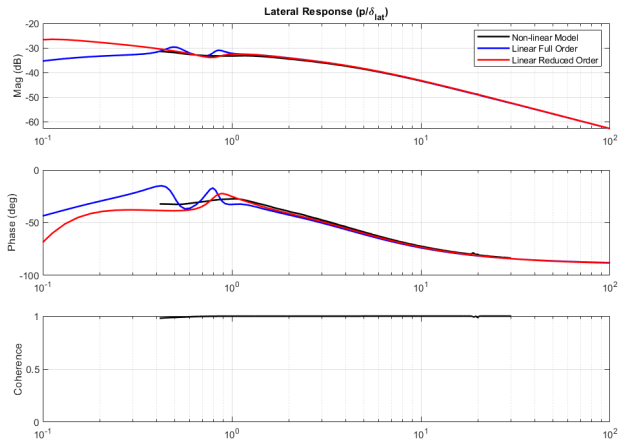

Figure 19: Torque-Controlled Lift+Cruise Frequency Response to Lateral Input at 40 Knots, P/δ_{lat}

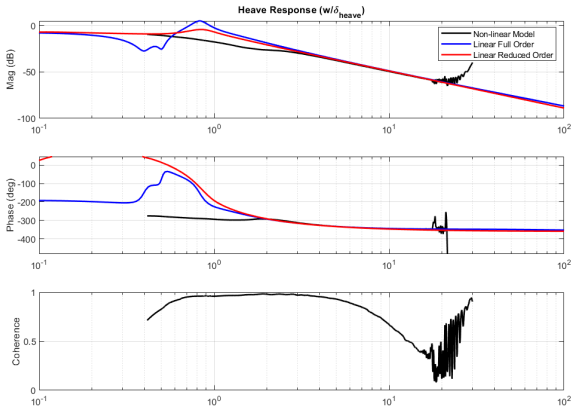

Figure 21: Torque-Controlled Lift+Cruise Frequency Response to Heave Input at 40 Knots, w/δ_{heave}

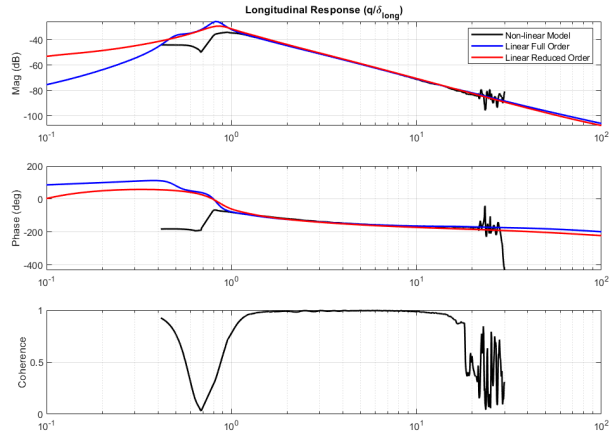

Figure 20: Torque-Controlled Lift+Cruise Frequency Response to Longitudinal Input at 40 Knots, Q/δ_{lon}

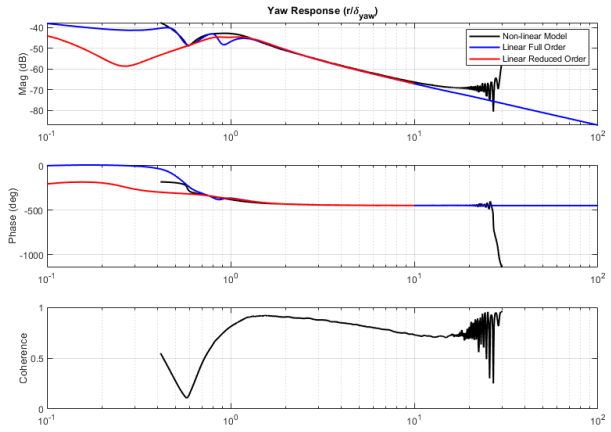

Figure 22: Torque-Controlled Lift+Cruise Frequency Response to Directional Input at 40 Knots, R/δ_{ped}

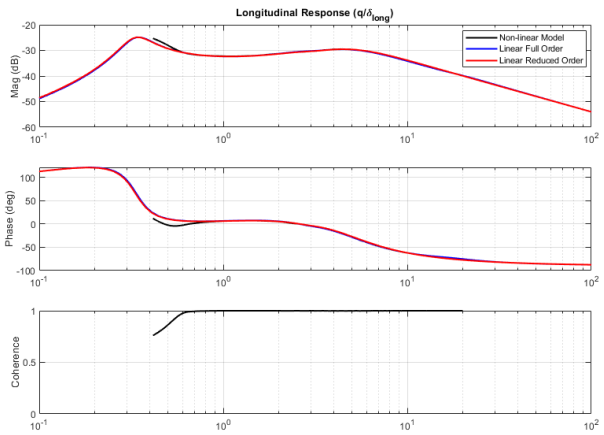

Figure 23: Torque-Controlled Lift+Cruise Frequency Response to Longitudinal Input at 120 Knots, Q/δ_{lon}

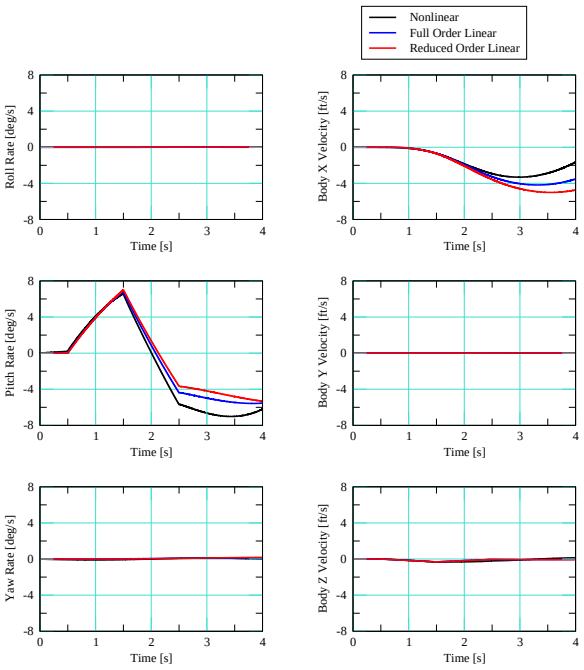

Figure 24: Tiltwing Doublet Response to Longitudinal Input at Hover

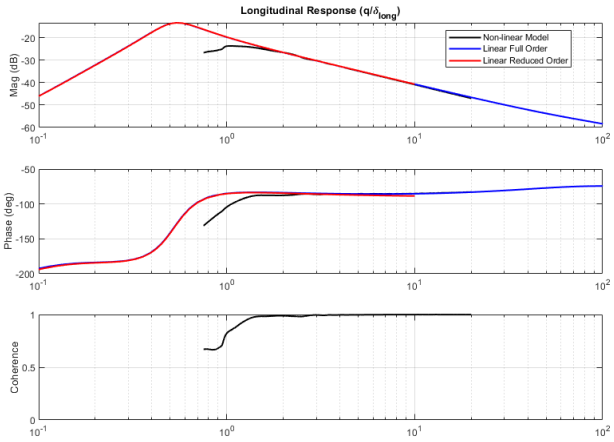

Figure 25: Tiltwing Frequency Response to Longitudinal Input at Hover, Q/δ_{lon}

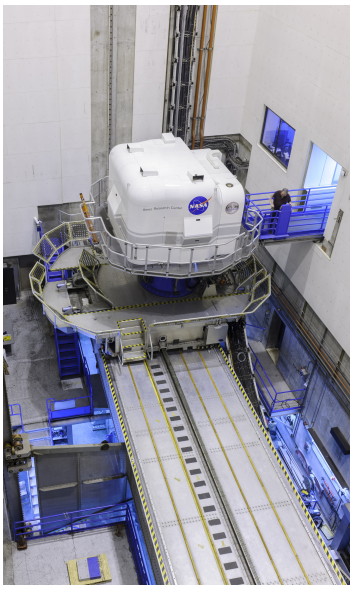

Figure 26: NASA Vertical Motion Simulator (credits: NASA/Dominic Hart)

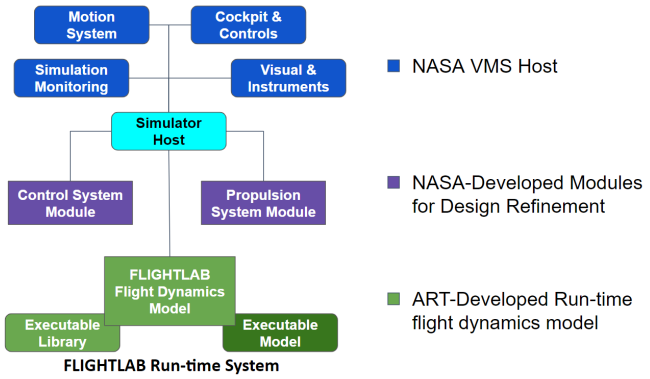

Figure 27: VMS Integration Communication Diagram

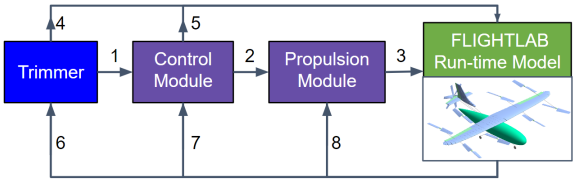

Figure 28: VMS Data Flow between Modules

(a) ART NovaSim Rig

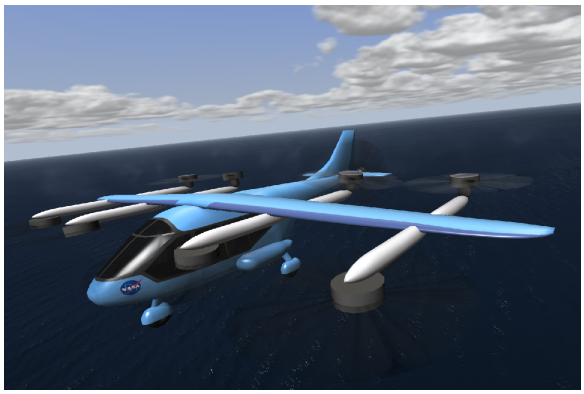

(b) Lift+Cruise in NovaSim Environment

Figure 29: Lift+Cruise Model Integration and Testing with the ART-NovaSim Environment